NF2/Merlin mediates contact-dependent inhibition of EGFR mobility and internalization via cortical actomyosin

Christine Chiasson-MacKenzie,[1,2,4] Zachary S. Morris,[1,2,4]* Quentin Baca,[5]* Brett Morris,[1,2,4]* Joanna K. Coker,[1,2,4] Rossen Mirchev,[5] Anne E. Jensen,[1,3] Thomas Carey,[1,3] Shannon L. Stott,[1,3,6] David E. Golan,[5] and Andrea I. McClatchey[1,2,4]

[1]Center for Cancer Research, [2]Department of Pathology, and [3]BioMEMs Resource Center, Massachusetts General Hospital, Charlestown, MA 02129
[4]Department of Pathology, [5]Department of Biological Chemistry and Molecular Pharmacology, and [6]Department of Medicine, Harvard Medical School, Boston, MA 02115

The proliferation of normal cells is inhibited at confluence, but the molecular basis of this phenomenon, known as contact-dependent inhibition of proliferation, is unclear. We previously identified the neurofibromatosis type 2 (NF2) tumor suppressor Merlin as a critical mediator of contact-dependent inhibition of proliferation and specifically found that Merlin inhibits the internalization of, and signaling from, the epidermal growth factor receptor (EGFR) in response to cell contact. Merlin is closely related to the membrane–cytoskeleton linking proteins Ezrin, Radixin, and Moesin, and localization of Merlin to the cortical cytoskeleton is required for contact-dependent regulation of EGFR. We show that Merlin and Ezrin are essential components of a mechanism whereby mechanical forces associated with the establishment of cell–cell junctions are transduced across the cell cortex via the cortical actomyosin cytoskeleton to control the lateral mobility and activity of EGFR, providing novel insight into how cells inhibit mitogenic signaling in response to cell contact.

Introduction

The failure to undergo contact-dependent inhibition of proliferation is a hallmark of tumor cells (Hanahan and Weinberg, 2011), but a mechanistic understanding of how normal cells stop dividing in response to cell–cell contact is lacking. Any mechanism of contact-dependent inhibition of proliferation must invoke the ability of cells to "sense" the degree of contact that they share with neighboring cells; whether this is achieved via the generation of contact-dependent biochemical and/or mechanical signals is unknown. Early studies of contact-dependent inhibition of proliferation concluded that the responsiveness of growth factor receptors on the cell surface, including the EGF receptor (EGFR), is inhibited by cell contact despite a continuous supply of ligand (McClatchey and Yap, 2012). Many studies have since supported the notion that signaling from various growth factor receptors is inhibited in response to cell contact, but the mechanistic basis for this is unknown.

The EGFR was the first discovered tyrosine kinase receptor and is a model for this critical class of mitogenic receptors (Lemmon and Schlessinger, 2010). EGFR signaling is initiated by ligand-induced conformational changes that facilitate dimerization, activation of the intracellular kinase domain, and recruitment of downstream effectors including components of the endocytic machinery (Lemmon and Schlessinger, 2010). Endocytosis has long been considered the definitive mechanism for negative regulation of activated EGFR, leading to pH-dependent dissociation of the receptor–ligand complex within endocytic vesicles (Avraham and Yarden, 2011). Prior to ligand dissociation, however, activated endosomal EGFR is sufficient to drive cell proliferation; in fact, internalization of ligand-bound receptor is necessary for the activation of major downstream EGFR signaling pathways (Lemmon and Schlessinger, 2010). If endocytosis were the principal mechanism for negatively regulating ligand-activated EGFR, the cell would be able to do so only after exposure to the potent signaling capacity of endosomal EGFR. Therefore, mechanisms

*Z.S. Morris, Q. Baca, and B. Morris contributed equally to this paper.

Correspondence to Andrea I. McClatchey: mcclatch@helix.mgh.harvard.edu

Abbreviations used in this paper: AJ, adherens junction; ANOVA, analysis of variance; CMV, cytomegalovirus; EGFR, EGF receptor; ERM, Ezrin, Radixin, and Moesin; HB, hepatoblast; LDC, liver-derived epithelial cell; MSD, mean square displacement; shSCR, scrambled short hairpin; SPTM, single-particle tracking microscopy; TJ, tight junction; TR-EGF, Texas red–labeled EGF; ZA, zonulae adherens.

The Rockefeller University Press $30.00
J. Cell Biol. Vol. 211 No. 2 391–405
www.jcb.org/cgi/doi/10.1083/jcb.201503081

likely exist that enable a cell to prevent EGFR signaling at the plasma membrane upon cell contact.

In previous studies, we identified the neurofibromatosis type 2 (NF2*)* tumor suppressor Merlin as a critical mediator of contact-dependent inhibition of proliferation and specifically of contact-dependent inhibition of EGFR internalization and signaling (Lallemand et al., 2003; Curto et al., 2007; Cole et al., 2008). These studies revealed that Merlin can block the internalization of activated EGFR in a contact-dependent manner via a mechanism that does not involve gross changes in ligand binding or in EGFR phosphorylation, localization, or bulk plasma membrane levels (Curto et al., 2007). Merlin is a unique type of tumor suppressor that localizes predominantly to the cell cortex and is closely related to the membrane–cytoskeleton linking proteins Ezrin, Radixin, and Moesin (ERMs; McClatchey and Fehon, 2009; Fehon et al., 2010). When activated, ERMs assemble multiprotein complexes at the plasma membrane via their N-terminal four-point-one ERM domain and link them to the cortical actin cytoskeleton via a C-terminal actin-binding domain (Fehon et al., 2010). In doing so, ERMs dynamically organize the morphological and mechanical properties of the cell cortex, as exemplified by their essential roles in building and elaborating the apical surface of epithelia and in driving increased cortical rigidity during mitotic rounding (McClatchey, 2014). Merlin lacks a C-terminal actin-binding domain but localizes to the cortical cytoskeleton and can interact directly with the actin-binding protein α-catenin (Gladden et al., 2010). In fact, a key function of Merlin is to limit the cortical distribution of Ezrin via a mechanism that involves α-catenin (Hebert et al., 2012). Localization of Merlin to the cortical cytoskeleton is necessary for contact-dependent inhibition of EGFR internalization, but the mechanism by which cortical Merlin controls EGFR is unknown (Cole et al., 2008). Importantly, pharmacologic EGFR inhibitors block the proliferation of *NF2*$^{-/-}$ primary and tumor cells in vitro and in vivo, suggesting that this mechanism is central to the tumor suppressor activity of Merlin (Morris and McClatchey, 2009; Benhamouche et al., 2010).

Membrane–cytoskeleton linking proteins such as Merlin/ERMs dynamically attach the cortical actomyosin cytoskeleton to the plasma membrane (Gauthier et al., 2012). The cortical cytoskeleton can thereby impact the dynamic distribution of plasma membrane receptors (Jaqaman and Grinstein, 2012). The cortical cytoskeleton is also physically and mechanically coupled to cell junctions that, in turn, transduce intercellular forces that enable cells to sense and respond to changes in their mechanical environment (Lecuit et al., 2011). It seems logical that these functions of the cortical cytoskeleton would be coordinated, but this has not been demonstrated. Mechanical forces experienced by cells within tissues can dramatically modulate cell signaling and behavior (DuFort et al., 2011). In fact, signaling downstream of EGFR is particularly sensitive to experimental manipulation of the mechanical forces that are transduced across cell junctions, but the molecular basis of this is not known (Kim et al., 2009; Kim and Asthagiri, 2011). Coordination between mechanosensing at cell junctions and control of receptors across the cortex is therefore a critical "black box" in our understanding of normal tissue morphogenesis and homeostasis and of how deregulation of cell and tissue architecture contributes to tumorigenesis.

Given its localization to the cortical actomyosin network, we hypothesized that Merlin may be central to a mechanism whereby mechanical signals are transduced from cell contacts across the cortex to regulate the dynamic distribution and internalization of EGFR. Here, we show that Merlin controls the properties of the cortical actomyosin network, which both immobilizes EGFR at the plasma membrane and stabilizes associated cell junctions in response to cell contact. In the absence of Merlin, ectopic apical Ezrin drives increased contractility of the cortical cytoskeleton, excess pulling on associated cell junctions, altered cortical Myosin IIA (MyoIIA) distribution, and a failure to inhibit EGFR internalization upon cell contact. These results uncover a novel mechanism of contact-dependent control of mitogenic signaling, provide new insight into the cortical function of Merlin, and suggest novel links between the control of cellular mechanics and receptor trafficking.

Results

Merlin is required for cytoskeleton- and signaling-dependent immobilization of apical EGFR in response to cell contact

Liver-derived epithelial cells (LDCs) from mice with a liver-specific *Nf2* deletion fail to undergo contact-dependent inhibition of proliferation (Curto et al., 2007; Cole et al., 2008). This overproliferation is associated with persistent internalization of activated EGFR and is blocked by EGFR inhibitors but not by elimination of Yap, the primary effector of the Hippo signaling pathway that can also be controlled by Merlin in some settings (Curto et al., 2007; Benhamouche et al., 2010; Boggiano and Fehon, 2012). Reintroduction of wild-type Nf2 (*Nf2*^{WT}) expression restores contact-dependent inhibition of EGFR internalization/signaling and proliferation (Curto et al., 2007; Cole et al., 2008).

Merlin associates with the cortical cytoskeleton, and this association is required for Merlin-dependent inhibition of EGFR internalization in contacting cells (Cole et al., 2008). Given that the cortical cytoskeleton can control membrane receptor lateral mobility, we hypothesized that Merlin might directly or indirectly regulate EGFR internalization by altering the dynamic distribution of receptor molecules to specific cytoskeletal and/or lipid compartments within the plasma membrane in response to cell contact. Therefore, we used single-particle tracking microscopy (SPTM) to examine Merlin-dependent effects on the mobility of individual EGFR molecules at the dorsal surface of *Nf2*$^{-/-}$ and *Nf2*^{WT}-expressing LDCs (Saxton and Jacobson, 1997; García-Sáez and Schwille, 2007). We found that in confluent *Nf2*^{WT}-expressing cells, the mean macro-diffusion coefficient (D_{macro}) of the total EGFR population was markedly decreased relative to that in *Nf2*$^{-/-}$ cells ($4.4 \pm 0.4 \times 10^{-12}$ cm^2 s^{-1} vs. $18 \pm 1.5 \times 10^{-12}$ cm^2 s^{-1}; $P = 4.6 \times 10^{-9}$), resulting in near-immobilization of the receptor (Fig. 1 A and Table S1). In contrast, nonconfluent *Nf2*^{WT}-expressing cells exhibited a moderate increase in the lateral mobility of EGFR relative to nonconfluent *Nf2*$^{-/-}$ cells (Fig. S1 A). The D_{macro} values that we observed in these experiments were comparable to those previously reported for EGFR lateral mobility in other epithelial cells (Kusumi et al., 1993). Like that prior study, we also observed heterogeneity in EGFR mobility. We found that SPTM datasets from our cells were best modeled as two distinct receptor subpopulations with Gaussian distributions of D_{macro} values—a slower moving, immobilized or confined subpopulation and a faster moving, freely diffusible subpopulation (Fig. 1 A).

To confirm that acute inactivation of endogenous Merlin led to similar changes in the lateral mobility and internaliza-

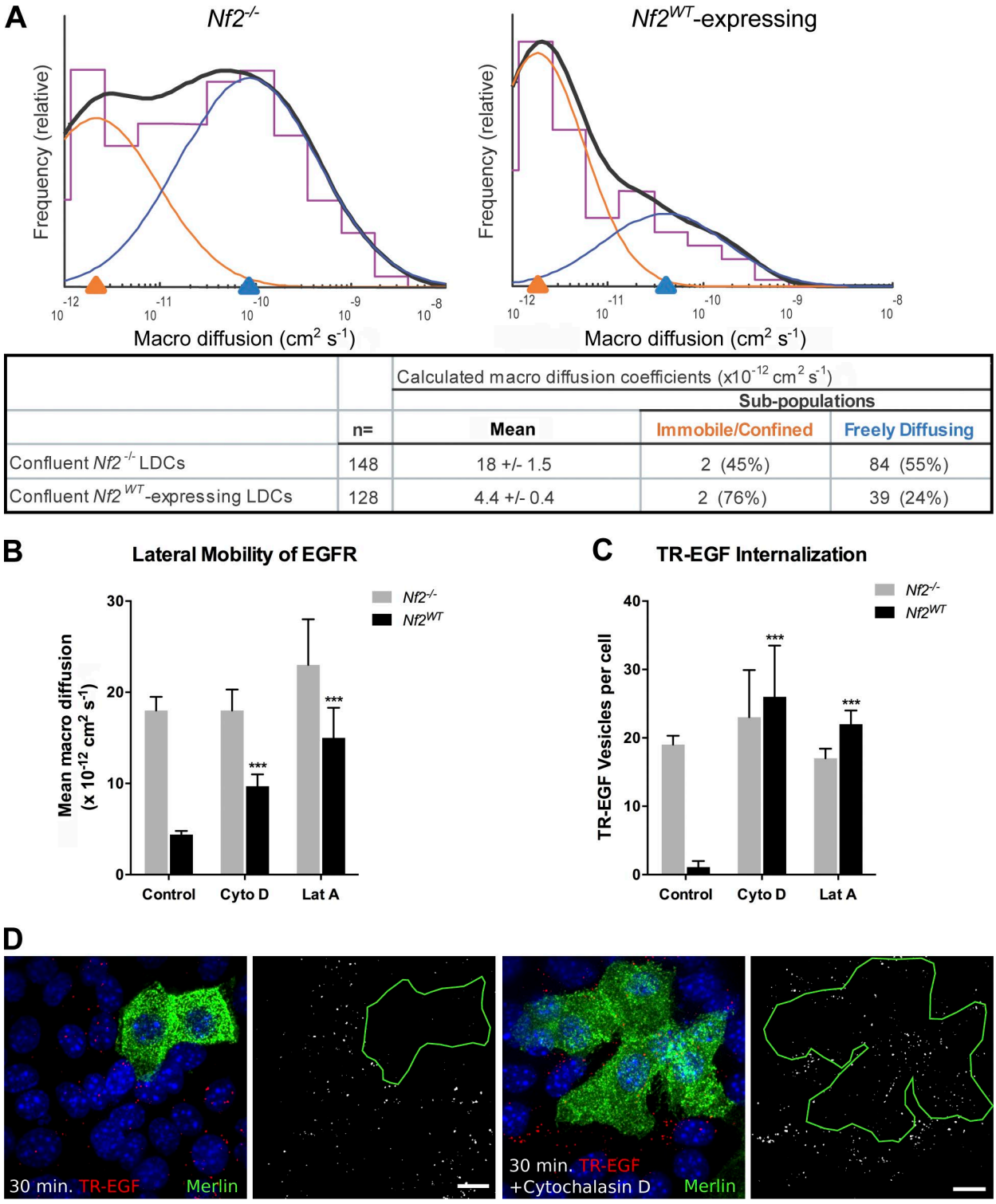

		Calculated macro diffusion coefficients (x10^{-12} cm^2 s^{-1})		
			Sub-populations	
	n=	Mean	Immobile/Confined	Freely Diffusing
Confluent *Nf2* $^{-/-}$ LDCs	148	18 +/- 1.5	2 (45%)	84 (55%)
Confluent *Nf2* ^{WT}-expressing LDCs	128	4.4 +/- 0.4	2 (76%)	39 (24%)

Figure 1. **EGFR is immobilized at the plasma membrane in a Merlin- and actin-dependent manner.** (A) SPTM depicting the mean diffusivity of EGFR molecules in the plasma membrane of *Nf2*$^{-/-}$ (left) or *Nf2*^{WT}-expressing (right) LDCs. Histograms (purple) show the relative frequency at which beads were observed (y axis) with a given coefficient (D_{macro}; x axis). Overlaid on each histogram is a two-Gaussian fit (orange and blue) and its sum (solid black). The log-scale x axis displays D_{macro} representing increasing lateral diffusivity from left to right. The underlying chart displays the log mean of D_{macro} ± SEM as well as the mean of the two-Gaussian fit subpopulations (right) and the percentage of receptors that fall into each subpopulation (parentheses). Subsequent figures show only the log mean of the D_{macro} ± SEM for comparison. Numerical values of calculated D_{macro} for all experiments are displayed in Table S1. (B) Lateral mobility of EGFR in *Nf2*$^{-/-}$ or *Nf2*^{WT}-expressing LDCs with and without 5-µM cytochalasin D or 5-µM latrunculin A treatment. (C) Internalization of TR-EGF, which reliably marks EGF–EGFR complexes in *Nf2*$^{-/-}$ or *Nf2*^{WT}-expressing LDCs with and without cytochalasin D or latrunculin A treatment. Numerical values for quantification of TR-EGF vesicles per cell for all experiments are displayed in Table S2. (D) Representative confocal images of internalized TR-EGF (red; 30-min stimulation) in mosaic populations of *Nf2*$^{-/-}$ and *Nf2*^{WT}-expressing (green) LDCs with and without cytochalasin D. Bars, 10 µm. (B and C) Data are represented as mean ± SEM. ***, P < 0.001 (one-way ANOVA with multiple comparisons). Data are representative of at least three experiments.

tion of EGFR, we eliminated Merlin acutely via adenoviral expression of the Cre-recombinase in primary $Nf2^{lox/lox}$ embryonic hepatoblasts (HBs). Comparison to wild-type HBs confirmed that endogenous *Nf2* expression was associated with a dramatic immobilization of EGFR and with blocked internalization of activated EGFR (monitored by Texas red–labeled EGF [TR-EGF]) at confluence (Fig. S1, B–D; Table S1; and Table S2). In contrast, $Nf2^{-/-}$ HBs exhibited persistent EGFR mobility and internalization at confluence (Fig. S1, B–D).

These results demonstrated a contact-dependent effect of Merlin on the lateral mobility of EGFR and confirmed that this regulation of EGFR occurs at the plasma membrane. In fact, by expressing a version of Merlin tagged with the c-Src myristoylation sequence for membrane localization ($Nf2^{myr}$), we confirmed that membrane-localized Merlin was sufficient for contact-dependent regulation of EGFR internalization (Fig. S2 A). Importantly, Merlin blocked TR-EGF internalization at all time points tested (Fig. S2 B), further supporting the notion that Merlin prevents EGFR internalization from the plasma membrane rather than altering the kinetics of endocytosis or stimulating rapid recycling or degradation of internalized receptors.

The lateral mobility of membrane receptors can be altered by the cortical cytoskeleton and/or sterol-rich microdomains of the plasma membrane (Lenne et al., 2006; Jaqaman and Grinstein, 2012). To determine whether Merlin-dependent immobilization of EGFR in confluent cells requires an intact cortical cytoskeleton, we examined the effects of latrunculin A and cytochalasin D, compounds that disrupt actin polymerization through distinct mechanisms, on EGFR mobility by SPTM (Wakatsuki et al., 2001). Treatment of confluent $Nf2^{WT}$-expressing cells with either compound effectively prevented EGFR immobilization; in contrast, neither agent significantly affected EGFR mobility in $Nf2^{-/-}$ cells (Fig. 1 B). Merlin-dependent inhibition of TR-EGF internalization in confluent cells was also reversed by latrunculin A and cytochalasin D (Fig. 1, C and D). Moreover, a mutant version of Merlin that specifically cannot localize to the cortical cytoskeleton ($Nf2^{18–595}$) failed to immobilize EGFR or block TR-EGF internalization (Fig. S2 C; Cole et al., 2008). In contrast, disruption of lipid rafts by depletion of membrane cholesterol with methyl-β-cyclodextrin (MβCD) did not prevent EGFR immobilization in confluent $Nf2^{WT}$-expressing cells (Fig. S2 D). These findings suggest that contact-dependent EGFR immobilization and inhibition of EGFR internalization depend on both the integrity of the cortical cytoskeleton and the ability of Merlin to interact with it.

To further understand the molecular basis of Merlin-mediated control of EGFR internalization, we asked whether this phenomenon was signaling dependent. We used SPTM to monitor the lateral mobility of receptors at the dorsal surface of confluent $Nf2^{-/-}$ and $Nf2^{WT}$-expressing cells that had been serum starved overnight. Strikingly, in aggregate receptor population analyses like those described in Fig. 1, we found no difference in EGFR mobility in $Nf2^{WT}$-expressing versus $Nf2^{-/-}$ cells upon initial exposure to EGF-labeled beads in serum-free media (Fig. 2 A, left). By 40–60 min, however, EGFR was completely immobilized in $Nf2^{WT}$-expressing cells, mirroring our previous SPTM measurements on confluent cells in 10% serum (Fig. 2 A, right). Importantly, this time-dependent effect of exposure to EGF-labeled beads was blocked by treatment

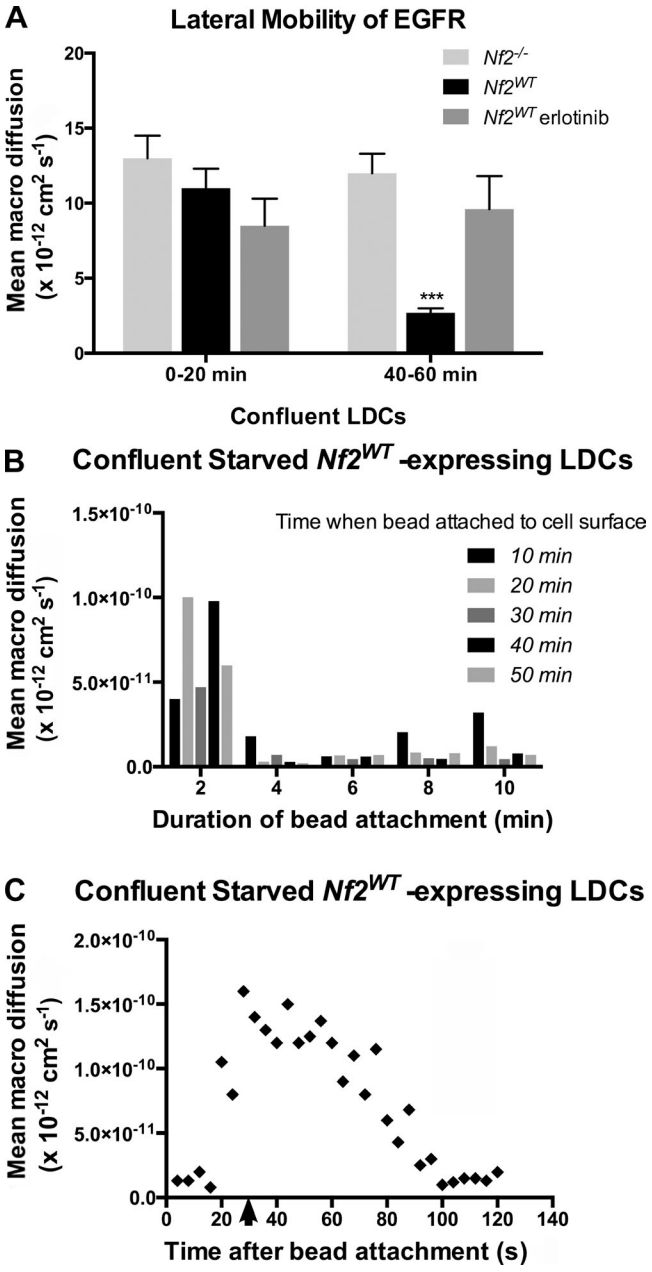

Figure 2. **Rapid, local, signal-dependent immobilization of EGFR in confluent $Nf2^{WT}$-expressing cells.** (A) Lateral mobility of EGFR in confluent, serum-starved $Nf2^{wt}$-expressing versus $Nf2^{-/-}$ LDCs at early (0–20 min) and late (40–60 min) time points after EGF-labeled beads were added. Also shown is the impact of 1-µM erlotinib treatment on EGFR mobility in $Nf2^{WT}$-expressing cells. Data are represented as mean ± SEM. ***, $P < 0.001$ (one-way ANOVA with multiple comparisons). (B) Lateral mobility of EGFR in confluent, serum-starved $Nf2^{WT}$-expressing LDCs measured at 2-min intervals after visually observing bead-to-cell attachment. Data are binned according to the time elapsed between exposing cells to EGF-labeled beads and observing bead-to-cell attachment. The graph shown is a representative time course of the mobility of a single bead over time. For each experiment, $n > 3$ beads. (C) Lateral mobility of single EGF-labeled beads on the surface of confluent, serum-starved $Nf2^{WT}$-expressing cells at increasing time points after release from a laser optical trap (arrow). Data are representative of at least three experiments.

with the EGFR inhibitor erlotinib; in the presence of erlotinib, EGFR was not immobilized in confluent *Nf2*^{WT}-expressing cells 40–60 min after exposure to EGF-labeled beads (Fig. 2 A). Furthermore, EGFR was not immobilized at any time point in *Nf2*$^{-/-}$ cells (Fig. 2 A).

Because of the lack of a time zero (t_0) for ligand binding in these population studies, this phenomenon could, in principle, reflect a global alteration of the cell cortex in response to the activation of individual receptors by ligand-conjugated beads (requiring >20 min). However, given the stoichiometry of binding of ligand-coated beads in these experiments (approximately one bead per cell), this explanation seemed unlikely, as such a pancellular response would require a dramatic amplification of very few receptor–ligand interactions for any given cell. Alternatively, differential receptor mobilities at 0–20 versus 40–60 min could reflect differences in the mean time elapsed since formation of the receptor–ligand complexes under observation. To determine whether time-dependent effects on receptor mobility in serum-starved *Nf2*^{WT}-expressing cells reflected a pancellular or local phenomenon, we measured the mobility of individual ligand-bound receptors every 2 min starting at a defined t_0 at which a bead was observed to associate with the receptor and assume a planar pattern of mobility. We found that regardless of when a receptor–ligand complex formed, the receptor initially displayed a significant degree of mobility and then was immobilized over a period of <4 min (Fig. 2 B). In a complementary approach, we used laser optical tweezers to place EGF-labeled beads on the dorsal surface of confluent, serum-starved *Nf2*^{WT}-expressing cells and monitor their mobility after release from the laser trap. After release, the beads initially assumed a freely diffusing lateral mobility followed by rapid immobilization over <100 s (Fig. 2 C). These data suggest that the contact-dependent regulation of EGFR by Merlin is also dependent on ligand-induced stimulation of EGFR kinase activity and may represent a mechanism of rapid feedback. Collectively, our findings indicate that Merlin inhibits the lateral mobility and internalization of activated EGFR at the plasma membrane in a rapid and localized manner in response to the establishment of cell contact.

Loss of Merlin yields increased mechanical stress at the apical junction

Merlin, like the ERMs, localizes to the cell cortex and to apical cell–cell junctions (Fig. S3 A; Cole et al., 2008) and is important for the integrity of mature adherens junctions (AJs; Lallemand et al., 2003; Gladden et al., 2010), raising the possibility that Merlin controls EGFR indirectly by stabilizing cell junctions. However, we recently found that a basic function of Merlin is to restrict the cortical distribution of Ezrin in single cells, suggesting that Merlin controls cortical cytoskeletal organization in the absence of cell junctions (Hebert et al., 2012). To define the relationship between cell contact and EGFR internalization, we examined cell junction establishment in LDCs, which are HB-like cells that establish immature AJs and do not form tight junctions (TJs) or apical microvilli (Curto et al., 2007). We found that in both *Nf2*$^{-/-}$ and *Nf2*^{WT}-expressing LDCs, AJ components form discrete linear cell–cell boundaries at early time points after establishing contact (Fig. 3, A and B; and Fig. S3 B). In contrast, at late confluence, AJs become disrupted, and AJ components are mislocalized in *Nf2*$^{-/-}$ but not *Nf2*^{WT}-expressing LDCs (Fig. 3, A and B; and Fig. S3 B). We hypothesized that Merlin-deficient AJs may be fragile as a result of a failure to stably associate with the actin cytoskeleton (Takeichi, 2014). Surprisingly, however, Merlin-deficient AJs recruit similar levels of actin, as well as a marked increase in vinculin, which is recruited to AJs as they experience elevated mechanical tension (Fig. 3, C–E; and Fig. S3 C; Yonemura et al., 2010). Moreover, reducing the mechanical stress on AJs via either treatment with the type II myosin inhibitor blebbistatin or culturing on soft hydrogels of defined stiffness (12 kPa; Fig. S3 D), which reduces junctional forces (Maruthamuthu et al., 2011), completely rescued late junction morphology (Fig. 3, F–H; and Fig. S3 E). Notably, pharmacologic inhibition of EGFR did not rescue junction integrity in *Nf2*$^{-/-}$ LDCs (Fig. S3 F). Together, these data suggest that loss of Merlin confers excess mechanical stress on AJs.

To corroborate these findings in a well-studied model of junction formation, we examined Caco2 colonic epithelial cells. Cultured Caco2 cells form a columnar monolayer with apical junctions that mature to form distinct circumferential zonulae adherens (ZAs) and apically positioned TJs (Otani et al., 2006; Leerberg et al., 2014). We previously found that Merlin is essential for organotypic cyst formation by Caco2 cells but did not investigate EGFR internalization or junction formation in these studies (Hebert et al., 2012). Therefore, we first established that EGFR internalization is regulated similarly in these cells. Indeed, TR-EGF internalization is inhibited in confluent Caco2 monolayers in the presence (cells expressing a scrambled short hairpin [shSCR]) but not absence (shNF2-expressing) of Merlin, despite equivalent levels of EGFR activation (Fig. 4, A and D; and not depicted). Furthermore, in control Caco2 cells, both the ZA and apically positioned TJ form concise linear intercellular boundaries, but loss of Merlin yielded a markedly sinuous junction morphology that was maintained at late confluence (Fig. 4, B, C, E, and F). Notably, this phenotype is distinct from that caused by experimentally interfering with AJ or TJ integrity in the same cells (Dunagan et al., 2012; Verma et al., 2012). Importantly, as in LDCs, blebbistatin treatment rescues junction morphology (Fig. 4, G and H). Thus, in two different types of epithelial cells, loss of Merlin is associated with a loss of contact-dependent regulation of EGFR internalization and with junctional changes that are caused by excess MyoII activity.

Increased medioapical contraction in confluent Merlin-deficient cells

Mechanical stress on apical junctions can be driven by circumferential contraction of the actomyosin belt at the ZA or by contraction of the medioapical cortical cytoskeleton, which exerts radial inward pulling forces upon the ZA (Martin and Goldstein, 2014). Both are well-studied mechanisms of apical constriction that drive tissue morphogenesis in other organisms, including *Drosophila melanogaster* and *Caenorhabditis elegans* (Martin and Goldstein, 2014). However, ZA contraction, which is driven by junctional Myosin II activity, is typically accompanied by a smooth ZA morphology (Hildebrand, 2005; Nishimura and Takeichi, 2008; Chua et al., 2009). In contrast, medioapical contraction, driven by Myosin II activity at the cell apex, applies force at discrete points along cell junctions, causing them to bend inward and adopt a junctional morphology similar to that of shNF2-expressing Caco2 cells (Martin et al., 2009). The altered junctional morphology apparent in the absence of Merlin could reflect a reorientation of forces from parallel to orthogonal, as would accompany medioapical contraction. In fact, in contrast to confluent control cells in which MyoIIA lo-

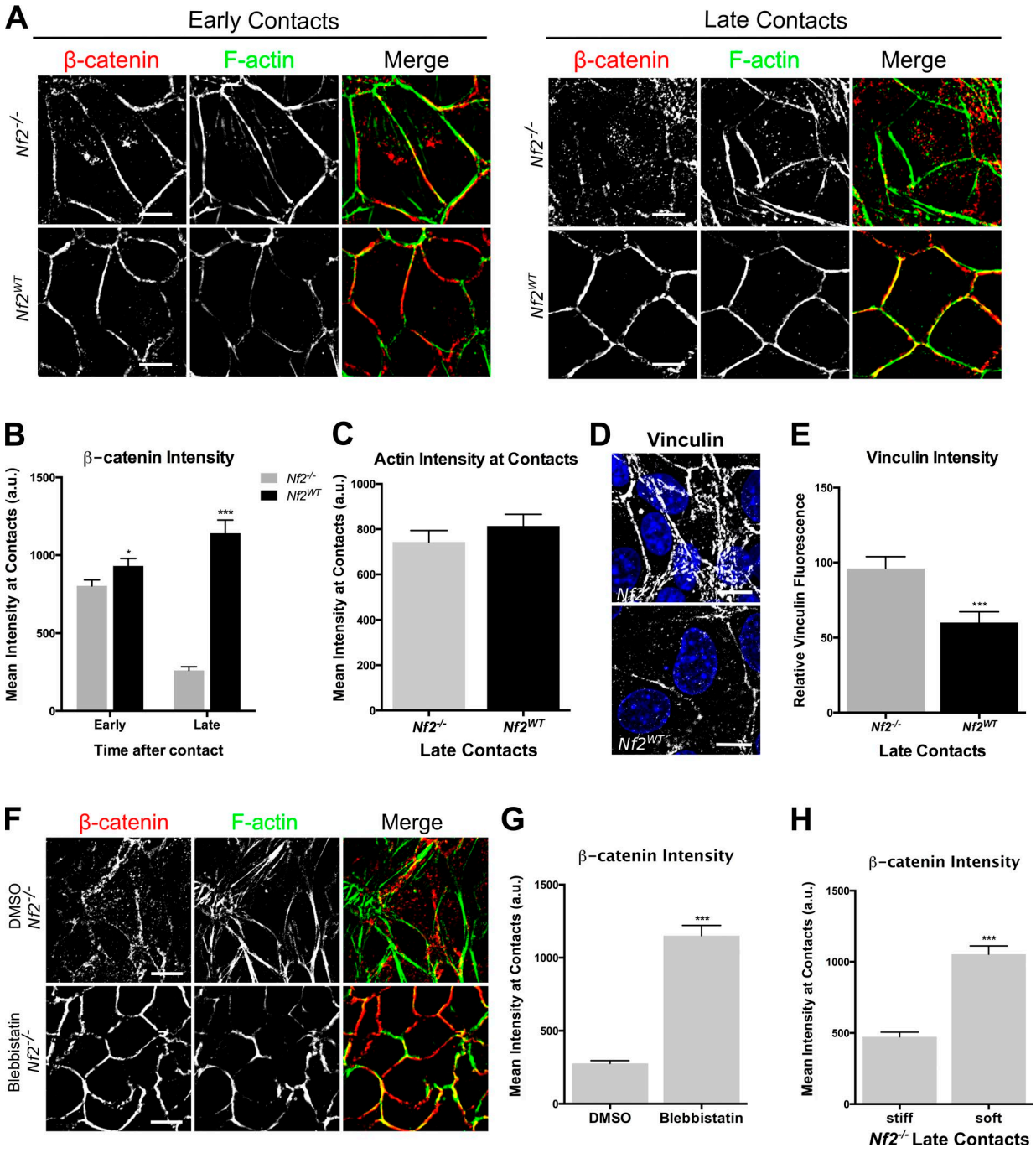

Figure 3. **Cell junctions in *Nf2*$^{-/-}$ LDCs are under increased mechanical stress.** (A) Confocal images showing *Nf2*$^{-/-}$ or *Nf2*^{WT}-expressing LDCs at early (left) and late (right) stages of confluence; cells were labeled with an anti–β-catenin antibody (red) and with phalloidin to detect F-actin (green). (B) Junctional localization of β-catenin was quantified by fluorescence intensity analysis of AJs in early and late confluent *Nf2*$^{-/-}$ and *Nf2*^{WT}-expressing LDCs. (C) Junctional localization of F-actin was quantified by fluorescence intensity analysis of AJs in late confluent *Nf2*$^{-/-}$ and *Nf2*^{WT}-expressing LDCs. (D) Confocal images showing endogenous vinculin at AJs in *Nf2*$^{-/-}$ and *Nf2*^{WT}-expressing LDCs. (E) The amount of vinculin at AJs in *Nf2*$^{-/-}$ and *Nf2*^{WT}-expressing LDCs was quantified by measuring the junctional area stained for vinculin. (F) Confocal images showing endogenous β-catenin (red) and/or F-actin (green) in *Nf2*$^{-/-}$ LDCs treated with 100-µM blebbistatin or vehicle (DMSO). (G) Junctional localization of β-catenin in DMSO- and blebbistatin-treated confluent *Nf2*$^{-/-}$ LDCs was quantified by fluorescence intensity analysis of AJs. (H) Junctional localization of β-catenin in *Nf2*$^{-/-}$ LDCs cultured on stiff (40 kPa) and soft (12 kPa) polyacrylamide hydrogels. (B, C, E, G, and H) Error bars indicate SEM (n = 25 junctions per group). *, P < 0.05; ***, P < 0.001. Data are representative of at least three experiments. Bars, 10 µm. a.u., arbitrary units.

calized to the ZA and uniformly across the medioapical cortex, MyoIIA formed condensed apical foci in Merlin-deficient cells that are strikingly reminiscent of the coalescence of apical Myosin II that is driven by centripetal cortical flow and accompanies medioapical contraction in flies (Fig. 5, A and B; Martin and Goldstein, 2014). Notably, actin was not strongly enriched in the MyoIIA foci (Fig. S4 A). Apical MyoIIA coalescence was also seen in *Nf2*$^{-/-}$ LDCs, which also exhibited increased cortical levels of activated myosin regulatory light chain, consistent with increased apical contractility (Fig. S4, B and E). In

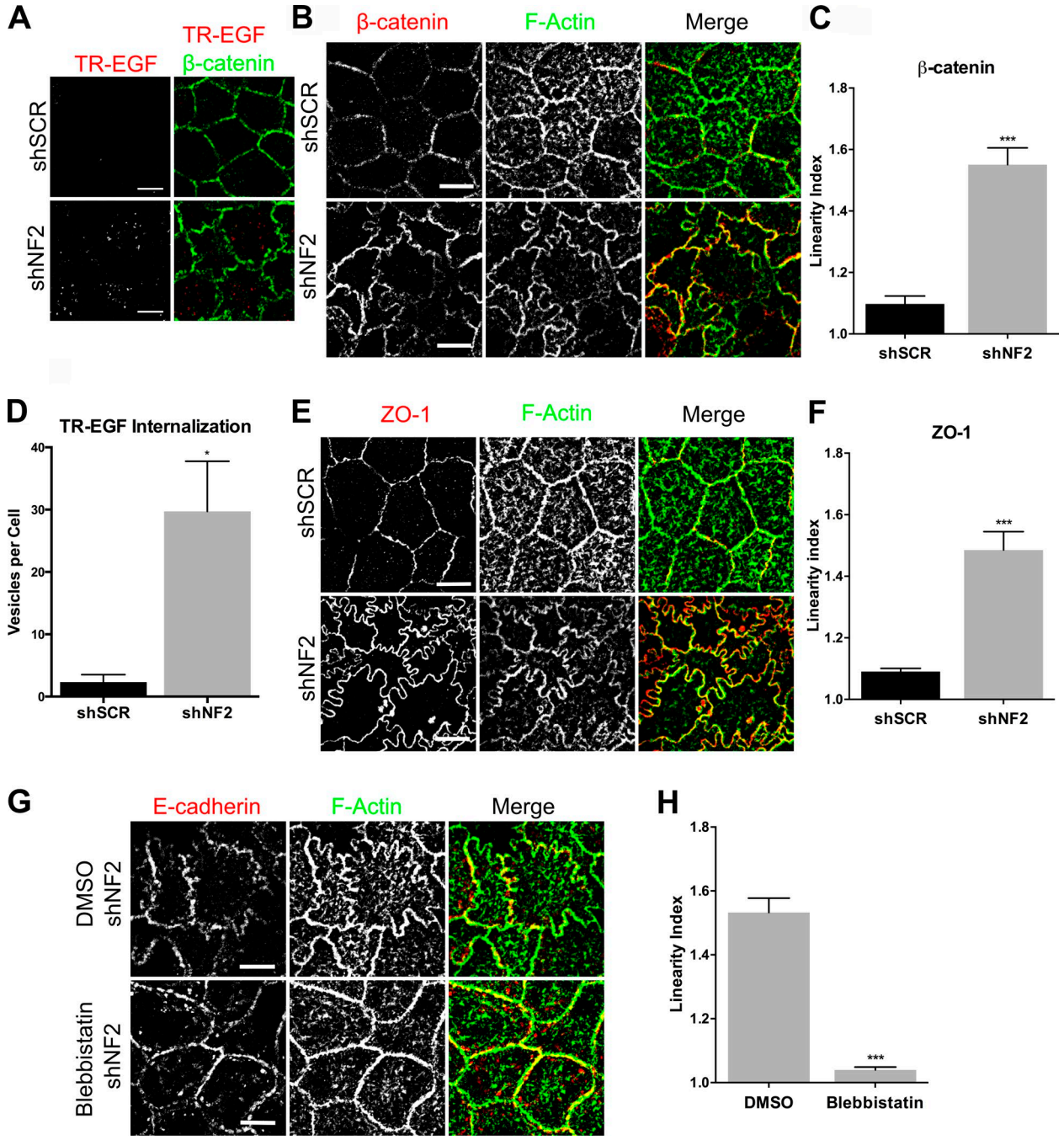

Figure 4. **Merlin limits EGFR internalization and junctional stress in Caco2 colonic epithelial cells.** (A) Confocal images of control (shSCR) and shNF2-expressing Caco2 cells showing the localization of β-catenin (green) and internalized TR-EGF (red; 30 min after stimulation). (B) Confocal images of control and shNF2-expressing Caco2 cells showing junctional localization of β-catenin (red) and F-actin (green). (C) Linearity index of β-catenin–labeled cell junctions in the experiment in B was quantified and graphed as the mean of the ratio of the length of a freehand-drawn line to a straight line drawn between two junctional vertices. (D) Internalized TR-EGF was quantified by fluorescence intensity thresholding to measure the number of TR-EGF vesicles per cell. (E) Confocal images showing junctional localization of ZO-1 (red) and F-actin (green). (F) Linearity index of ZO-1–labeled junctions calculated from the experiment in E. (G) Confocal images of shNF2-expressing Caco2 cells treated with 100-µM blebbistatin or DMSO showing junctional localization of E-cadherin (red) and F-actin (green). (H) Linearity index of F-actin–labeled junctions calculated from the experiment in F. (C, D, F, and H) Error bars indicate SEM. *n* = at least 25 junctions per group. *, $P < 0.05$; ***, $P < 0.001$. Data are representative of at least three experiments. Bars, 10 µm.

contrast, the distribution of Myosin IIB was similar in wild-type and Merlin-deficient cells of both types (Fig. 5 F and Fig. S4 C).

Apical constriction in *Drosophila* ventral furrow cells is accompanied by an apical shift and vertical shortening of the apical junction that is thought to be caused by increased medioapical pulling (Dawes-Hoang et al., 2005). We suspected that, as during apical constriction, MyoIIA foci form as a result of a ratchet-like mechanism that reflects apically restricted cortical pulling against stable apical junctions. Indeed, we found that Merlin-deficient junctions were condensed vertically at the apical junction complex, rather than evenly distributed along the lateral boundary, despite the fact that shNF2-expressing cells

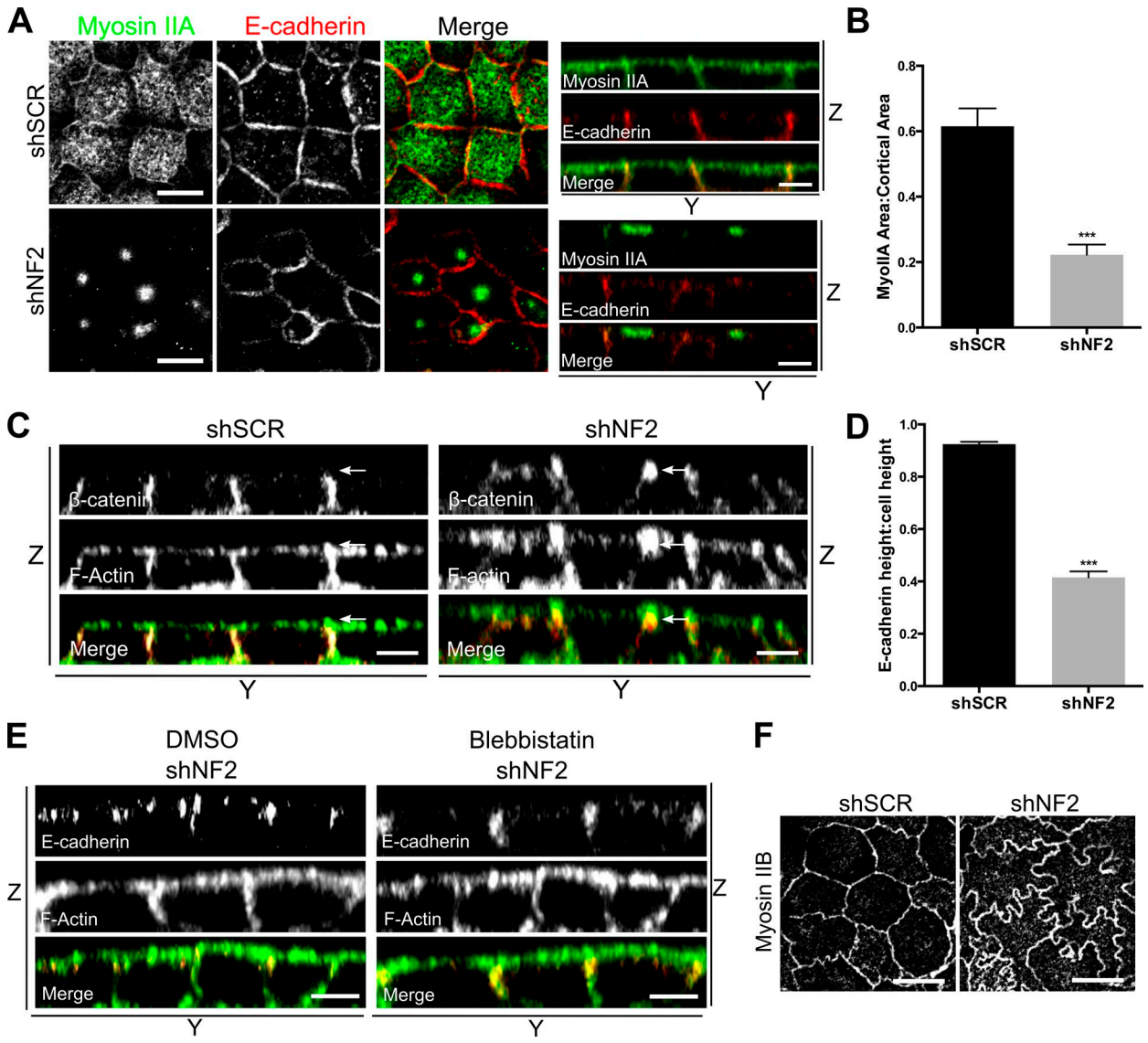

Figure 5. **Features of apical contraction in Merlin-deficient cells.** (A) Confocal images showing the cortical distribution of MyoIIA (green) and E-cadherin (red) in control (shSCR) and shNF2-expressing Caco2 monolayers. Bars, 10µm. The distributions of E-cadherin and F-actin along the z axis are shown in accompanying y-z views (apical = top). Bars, 5µm. (B) The cortical area covered by MyoIIA was quantified by calculating the ratio of cortical MyoIIA to the total cortical area delimited by F-actin. n = 25 cells per group. (C) Y-Z confocal images of control and shNF2-expressing Caco2 cells showing the vertical height and apical position of the ZA marked by β-catenin and F-actin. Arrows indicate the apical junction region. Bars, 5µm. (D) Ratio of E-cadherin–marked cell junction height to total cell height in control and shNF2-expressing Caco2 cells. n = 10 cells per group. (E) Y-Z confocal images depicting the vertical height and position of the E-cadherin and F-actin–stained ZA in shNF2-expressing Caco2 cells treated with either 100-µM blebbistatin or DMSO. Bars, 5µm. (F) Confocal images showing the distribution of Myosin IIB in control and shNF2-expressing Caco2 cells. Bars, 10µm. Error bars indicate SEM. ***, $P < 0.001$. Data are representative of at least three experiments.

exhibit a slightly greater average cell height (Fig. 5, C and D). Notably, this aspect of Merlin-deficient AJs was also rescued by blebbistatin, confirming that it is also a consequence of excess mechanical force (Fig. 5 E). Together, these data are consistent with a model wherein loss of Merlin drives increased medioapical contraction, MyoIIA coalescence, and excess mechanical pulling forces on the ZA.

Apical MyoIIA is required for contact-dependent inhibition of EGFR internalization

Loss of the uniform distribution of apical MyoIIA in favor of coalesced apical foci correlates with persistent TR-EGF internalization at confluence in Merlin-deficient LDCs and Caco2 cells (Fig. 5 A and Fig. 4 A). Indeed, blebbistatin treatment of established Merlin-deficient monolayers rescues junction morphology (Fig. 4, G and H) but does not restore MyoIIA cortical distribution or block TR-EGF internalization in either cell type (Fig. 6, A and B; and Fig. S4 B). This suggests that uniformly distributed cortical MyoIIA activity is essential for the inhibition of EGFR internalization in confluent control cells. In fact, we identified a strong anticorrelation between TR-EGF internalization and the cortical area covered by MyoIIA in control populations (Fig. 6 C). To further test this, we inhibited Myosin II activity in confluent wild-type Caco2 monolayers. Although blebbistatin had no apparent effect on the ZA or on MyoIIA distribution, it completely reversed the inhibition of TR-EGF internalization, mimicking the effect of Merlin deficiency (Fig. 6, D and E). Together, these data suggest that in

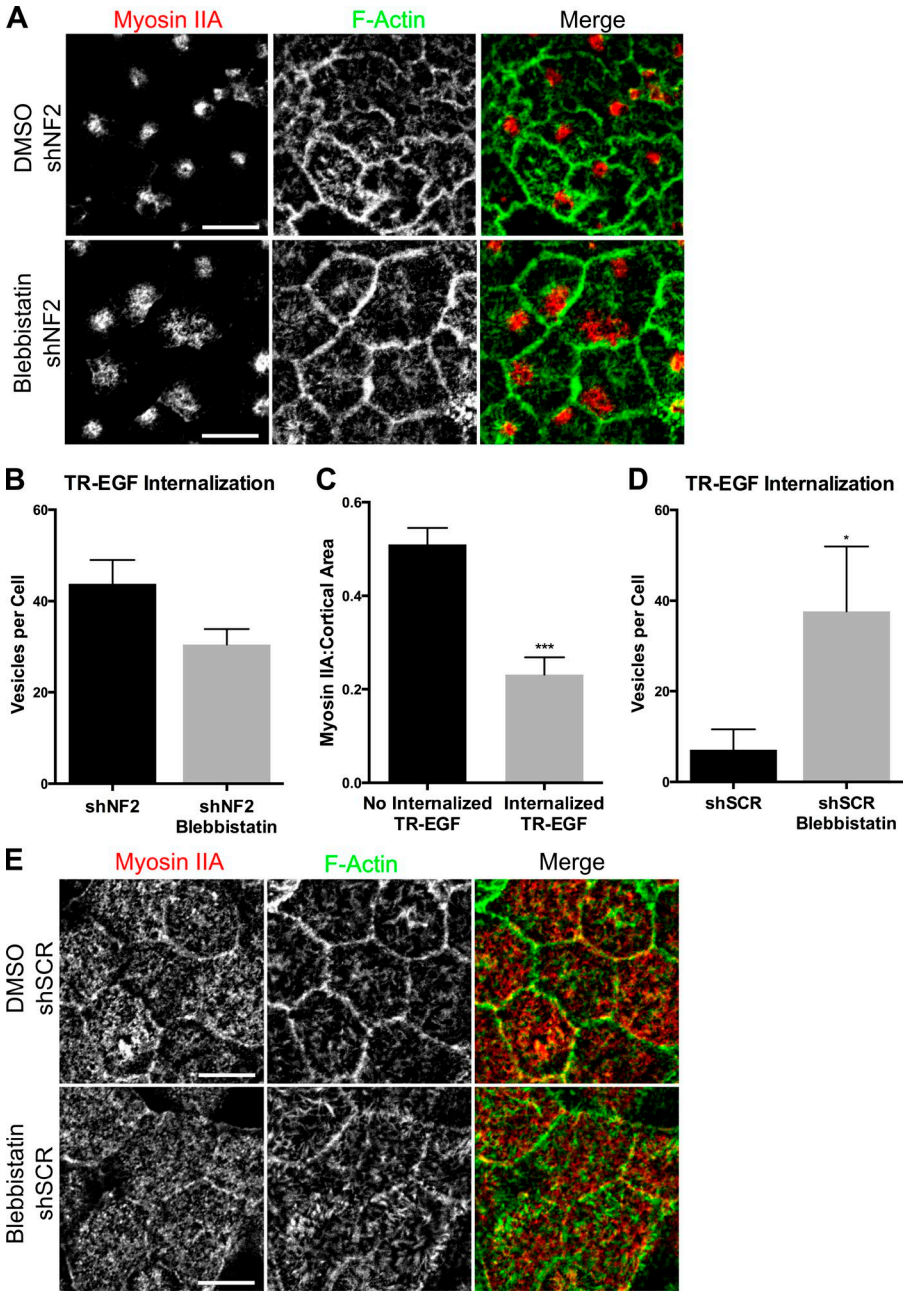

Figure 6. **Uniformly distributed MyoIIA is essential for contact-dependent inhibition of EGFR internalization.** (A) Confocal images of shNF2-expressing cells treated with 100-µM blebbistatin or DMSO and stained for MyoIIA and F-actin. (B) Quantification of internalized TR-EGF–containing vesicles (30 min after stimulation) in DMSO and blebbistatin-treated shNF2-expressing cells. *n* = >50 cells per group. P > 0.05. (C) Graph shows the fraction of cortical area covered by MyoIIA in shSCR cells that do not (left) versus do (right) display internalized TR-EGF at 30 min after stimulation. *n* = 25 cells per group. (D) Internalized TR-EGF (30 min after stimulation) was quantified in DMSO and blebbistatin-treated control cells. *n* = >50 cells per group. (E) Confocal images depict MyoIIA and junctional F-actin localization in control Caco2 cells treated with DMSO or 100-µM blebbistatin. Error bars indicate SEM. *, P < 0.05; ***, P < 0.001. Data are representative of at least three experiments. Bars, 10 µm.

normal cells, maintenance of active MyoIIA across the cortical cytoskeleton in response to cell–cell contact is required for immobilizing EGFR and blocking EGFR internalization. Conversely, the restriction of apical MyoIIA into cortical foci in the absence of Merlin eliminates the MyoIIA-dependent block of EGFR internalization.

Ectopic apical Ezrin in confluent Merlin-deficient cells

Increased medioapical contractility in Merlin-deficient cells could be caused by increased membrane tension (Gauthier et al., 2012). The ERM proteins are well-established membrane–cytoskeleton cross-linking proteins that drive increased membrane tension and contractility during mitotic rounding in fly and mammalian cells (Carreno et al., 2008; Kunda et al., 2008; Luxenburg et al., 2011). In fact, our earlier studies revealed that a key consequence of Merlin loss in Caco2 cells, and in several tissues in vivo, is increased cortical Ezrin (Hebert et al., 2012). In Caco2 monolayers, Ezrin is restricted to the apical surface; therefore, we asked whether excess Ezrin at the apical cortex is a feature of confluent Merlin-deficient monolayers. Indeed, we found that the levels of apical Ezrin are markedly increased in shNF2-expressing Caco2 cells and in *Nf2*$^{-/-}$ LDCs, which also exhibit increased levels of activated ERM (pERM; Fig. 7, A and B; and Fig. S5, A and B). Activation of Ezrin/ERMs in control cells using the cell-permeable phosphatase inhibitor Calyculin A, which drives Ezrin/ERM phosphorylation (Kunda et al., 2008; Viswanatha et al., 2012), promotes MyoIIA coalescence and sinuous junction morphology, mirroring Merlin deficiency (Fig. 7, C–F). Moreover, depletion of Ezrin in shNF2-expressing Caco2 cells completely rescues both junction morphology and MyoIIA distribution, demonstrating that excess Ezrin drives the cortical and junction defects observed in Merlin-deficient cells (Fig. 7, G–I; and Fig. S5 C). Finally,

in confluent control cultures, we occasionally observed cells with sinuous junctions that mirrored those of shNF2-expressing Caco2 cells; closer inspection revealed that these cells were mitotic and also exhibited increased apical Ezrin (Fig. S5 C). The apical surface of mitotic cells was constricted relative to neighboring cells, with the bulging mitotic equator positioned beneath the apical surface of the monolayer. These data are consistent with a model whereby in the absence of Merlin, increased apical Ezrin drives medioapical contraction, MyoIIA redistribution, loss of actomyosin-mediated EGFR immobilization, and persistent internalization of, and signaling from, ligand-bound EGFR at confluence.

Discussion

Our study indicates that mechanical forces associated with the establishment of cell–cell junctions are transduced across the cell cortex via the cortical actomyosin cytoskeleton to control the mobility and activity of plasma membrane receptors. For EGFR, the consequence of this contact-dependent control is actin- and MyoII-dependent immobilization at the cortex, which prevents internalization and recruitment of downstream signaling effectors (Curto et al., 2007). Importantly, this mechanism of control also requires EGFR kinase activity, suggesting that in contacting cells activated EGFR recruits an alternative effector that both immobilizes EGFR and impedes its association with canonical effectors, such as Grb2 and Cbl, that drive endocytosis and mitogenic signaling. Notably, there are intriguing parallels between our study and that of Lidke et al. (2005), who showed that EGFR associates with filopodial actin and is transported by retrograde flow toward the cell body via a mechanism that requires EGFR kinase activity; once activated EGFR dimers reach the cell body they are endocytosed, which would enable mitogenic signaling (Lemmon and Schlessinger, 2010). Although the mechanism by which EGFR communicates with actin filaments in filopodia is not known, elimination of actin treadmilling immobilized filopodial EGFR in that study (Lidke et al., 2005). We propose that the association of EGFR with a mechanically immobilized cortical cytoskeleton in contacting cells could proceed via a similar mechanism. The requirement for EGFR kinase activity for contact-dependent control suggests that this mechanism may be unique to EGFR or to a subset of receptors that, when activated, can recruit such actin-associating effectors.

Merlin itself could link EGFR to a cortical cytoskeleton that has been mechanically stabilized in response to cell contact via the PDZ domain–containing adapter NHERF1 (Curto et al., 2007). Alternatively, the primary effect of Merlin could be to alter the configuration of the cortical cytoskeleton itself, thereby facilitating the appropriate distribution and activation of MyoIIA and other factors that immobilize EGFR and limit medioapical contraction at confluence. Most interesting is the possibility that Merlin simultaneously alters the actin cytoskeleton and links EGFR to it via NHERF1; indeed, the closely related ERM proteins seem designed to simultaneously link membrane complexes to, and alter the properties of, the cortical cytoskeleton (Fehon et al., 2010; McClatchey, 2014).

Merlin could alter the configuration of the cortical cytoskeleton in two nonexclusive ways: (1) by limiting cortical Ezrin and (2) by controlling the activity of the actin-binding protein α-catenin, with which Merlin directly interacts (Gladden et al., 2010). Although best known for its mechanosensitive role in linking the AJ to the actin cytoskeleton, mounting evidence indicates that α-catenin can remodel actin away from cell junctions (Lien et al., 2008; Benjamin et al., 2010; Buckley et al., 2014). Most recently, it has been shown that α-catenin binds cooperatively to, and alters the conformation of, actin filaments, impeding the loading of other actin-modifying proteins (Hansen et al., 2013). Merlin and α-catenin stabilize each other at the cortex of single cells, and α-catenin loss mimics Merlin loss in single cells, yielding ectopic cortical Ezrin (Hebert et al., 2012); therefore, Merlin restricts cortical Ezrin via a mechanism that involves α-catenin. An intriguing possibility then is that Merlin facilitates α-catenin–dependent remodeling of actin filaments, which in turn impedes the association of Ezrin. Such a mechanism could explain the propagation of mechanical signals from the AJ/ZA, where α-catenin mechanosensitively links junction complexes to the cortical cytoskeleton, across the cortex.

Our data best fit a model wherein the primary consequence of Merlin loss is excess medioapical contraction, which causes secondary defects in apical cell junctions. The coalescence of apical MyoIIA, together with both planar and vertical aspects of junction morphology, mirror that of established examples of medioapical contraction (Martin and Goldstein, 2014), and both junctional phenotypes are rescued by blebbistatin treatment. Medioapical and junctional forces must be balanced in order to maintain proper intrajunctional tension and monolayer integrity, although how this coordination is achieved remains to be defined (Wu et al., 2014). Merlin, Ezrin, and α-catenin all localize to both the medioapical cortex and to apical junctions, and mutants that distinguish these localizations have not been identified; therefore, we cannot rule out contributions of junctional Merlin/Ezrin/α-catenin to maintaining this balance. Indeed, the apical junction and medioapical cortex are perhaps best thought of as a continuum, and the dual localization of proteins like Merlin/Ezrin/α-catenin and actin itself is likely central to the ability of cells to sense and respond to cell contact. Our data argue that increased medioapical contraction in the absence of Merlin is driven by Ezrin-induced changes in the configuration of the cortical cytoskeleton. In mitotic cells, elevated cortical Ezrin increases cortical rigidity by increasing local actin filament concentration and MyoII accumulation (Carreno et al., 2008; Kunda et al., 2008; Luxenburg et al., 2011). In the absence of Merlin, an increase in cortical Ezrin, specifically across the apical surface, could similarly drive minifilament formation, actomyosin flow, and excess medioapical contraction (Lecuit et al., 2011; Martin and Goldstein, 2014).

Our studies also have important translational implications for *NF2* mutant tumors. First, deregulation of this mechanism of EGFR control may be an important driver of NF2-associated tumorigenesis. Indeed, pharmacologic EGFR inhibitors block the proliferation of neoplastic cells in *Nf2* mutant mouse kidney and liver tumors (Morris and McClatchey, 2009; Benhamouche et al., 2010). Other receptors that are subject to this Merlin- and contact-dependent control mechanism may be additional drivers of *NF2* mutant tumors or molecular escape pathways upon EGFR inhibition. Second, basic insight into the role of Merlin in controlling the cortical cytoskeleton will inform our understanding of how Merlin controls other pathways including the Hippo pathway, which is also sensitive to changes in the mechanical cellular environment (Boggiano and Fehon, 2012). In fact, our work suggests that EGFR and Hippo signaling may be coordinated in response to changes in the mechanical forces experienced by cells.

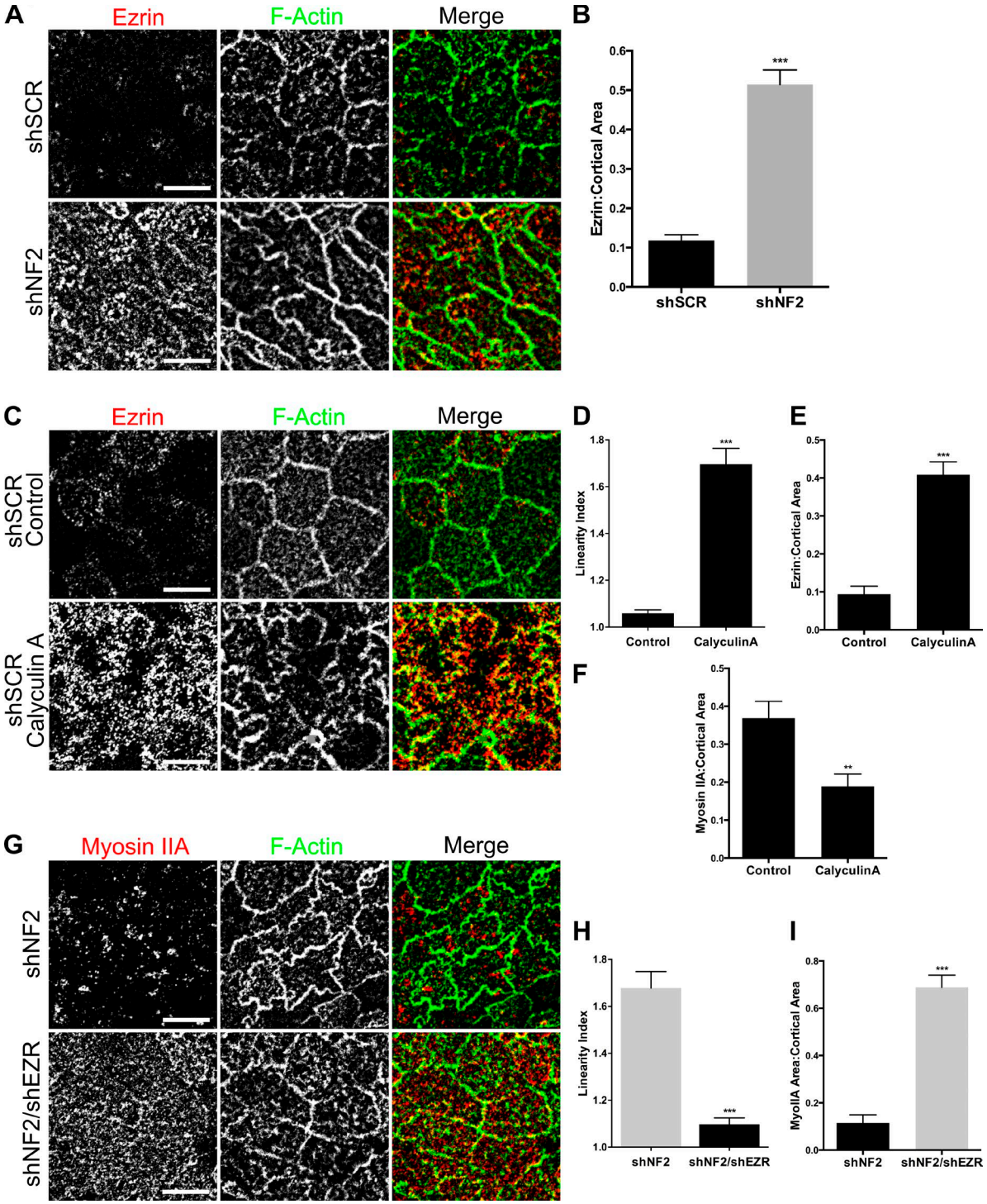

Figure 7. **Increased cortical Ezrin drives apical contractility.** (A) Endogenous Ezrin (red) and junctional F-actin (green) in confluent control and shNF2-expressing Caco2 cells as depicted by representative confocal images. (B) The levels of apical Ezrin in A were quantified by calculating the ratio of apical Ezrin to the total apical area delimited by F-actin. (C) Confocal images showing apical Ezrin and junctional F-actin in shSCR Caco2 cells treated with DMSO or 1-µM calyculin A for 5 min. (D) Linearity index of F-actin–labeled junctions calculated from the experiment in C. (E) Levels of apical Ezrin in control or calyculin A–treated cells. (F) Levels of cortical MyoIIA in control or calyculin A–treated cells. (G) Confocal images depict the levels and distribution of MyoIIA (red) and F-actin (green) in shNF2- and shNF2/shEZR-expressing Caco2 cells. (H) Linearity index in shNF2- and shNF2/shEZR-expressing cells. (I) Cortical area covered by MyoIIA in shNF2- and shNF2/shEZR-expressing cells. Error bars indicate SEM. **, P < 0.01; ***, P < 0.001. Data are representative of at least two experiments. Bars, 10 µm.

Finally, the demonstration that the transduction of mechanical forces experienced at cell junctions can influence plasma membrane receptors across the cell cortex strongly suggests that changes in the external mechanical environment will have a strong impact on receptor signaling. Indeed, EGFR signaling is known to be sensitive to changes in the mechanical forces experienced across cell junctions (Kim et al., 2009; Kim and Asthagiri, 2011). Our studies suggest that apical constriction

and EGFR trafficking could be coordinated in normal tissues, for example during the programmed changes in apical expansion/constriction that intestinal epithelial cells undergo during morphogenesis and homeostasis (van der Flier and Clevers, 2009). Our studies also predict that the mechanical environment will markedly impact the contribution of EGFR signaling to tumorigenesis as well as the sensitivity of cells to pharmacologic inhibitors of EGFR or other mechanosensitive receptors. Alterations in cell and tissue architecture are universal and early features of developing tumors, and mounting evidence indicates that the mechanical forces experienced by cells within a tumor are very different from those in normal tissues (Huang and Ingber, 2005; DuFort et al., 2011; Kraning-Rush and Reinhart-King, 2012). Moreover, most preclinical studies of drug sensitivity and resistance are performed in cells cultured in polystyrene dishes, which are >1,000× stiffer than normal tissues (Kraning-Rush and Reinhart-King, 2012) and may therefore not accurately predict tumor cell drug sensitivity. Thus, knowledge of the impact of the mechanical environment on EGFR signaling and drug sensitivity may be essential toward predicting their clinical value in patients.

Materials and methods

Cell culture and reagents

LDCs are HB-like cells derived from early hyperproliferative lesions arising in *Alb-Cre;Nf2$^{lox/lox}$* mice. *Alb-Cre;Nf2$^{lox/lox}$* mice were generated by crossing homozygous *Nf2$^{lox/lox}$* mice (FVB/N) with transgenic mice expressing the Cre-recombinase gene under a liver-specific albumin promoter (Alb-Cre; B6.Cg-Tg[Alb-cre]21Mgn/J; The Jackson Laboratory; Giovannini et al., 2000; Postic and Magnuson, 2000). To isolate cells, the liver of a 12-wk-old *Alb-Cre;Nf2$^{lox/lox}$* mouse was removed, minced, dissociated in Liver Dissociation Medium (Invitrogen), and cultured in 10% FBS-DMEM. Clonal cell lines were established by limiting dilution (Curto et al., 2007; Benhamouche et al., 2010). Wild-type embryonic HBs were isolated from the livers of embryonic day (E) 14.5 *Nf2$^{lox/lox}$* embryos as described for LDCs. HBs were plated on type I collagen (BD)–coated dishes in F12-DMEM medium supplemented with 10% FBS, 100 ng/ml EGF, 60 ng/ml IGF-II, and 10 mg/ml insulin. Once epithelial clones appeared, several were isolated using cloning cylinders and further expanded (Benhamouche et al., 2010). *Nf2* deletion in cultured HBs was achieved via infection with adenoviral Cre-recombinase (Ad5CMV-Cre) as described previously (Lallemand et al., 2003). Human Caco2 cells were a gift from W. Lencer (Boston Children's Hospital, Boston, MA). AD-293 cells for adenovirus production were purchased from Agilent Technologies, and 293T cells for retrovirus and lentivirus production were purchased from ATCC. Cells were cultured in DMEM containing 10% FBS and 1% penicillin/streptomycin.

The following conditions were used for pharmacological treatments (duration of treatment before start of the experiment): cytochalasin D (Sigma-Aldrich), 5 µM for 30 min; latrunculin A (Cayman), 5 µM for 30 min; methyl-β-cyclodextrin (Sigma-Aldrich), 10 mM for 45 min; blebbistatin (EMD Millipore), 100 µM for 30 min; erlotinib (ChemieTek), 1 µM for 120 min; BIBW-2992 (Selleck), 1 µM for 60 min; and calyculin A (Sigma-Aldrich), 1 µM for 5 min. Treatment was continued at the stated doses for the duration of the experiment.

Plasmids and shRNA constructs

Merlin expression constructs (*Nf2^{WT}* and *Nf2$^{18–595}$*) were generated by PCR amplification of the mouse *Nf2* coding region (Lallemand et al., 2003; Cole et al., 2008). Human NF2^{myr}, containing the c-src myristoylation sequence for membrane targeting, was a gift from H. Morrison (Leibniz Institute, Jena, Germany). The C-terminal myc tag was removed by PCR (Hebert et al., 2012). Constructs were cloned into the pBABE or pAdCMV vectors under the control of a cytomegalovirus (CMV) promoter. Lentiviral shRNA constructs targeting human NF2 (5′-GAGGAAGCAACCCAAGACGTT-3′) or a scrambled control (shSCR; 5′-CAGTCGCGTTTGCGACTGG-3′) in a pLKO-puro.1 vector under the control of the human U6 promoter were gifts from M. James (Massachusetts General Hospital, Boston, MA; James et al., 2008). The shRNA construct targeting human Ezrin (5′-TTGATTCC ATACATTTCCAGG-3′) in a pLKO-puro.1 vector was purchased from GE Healthcare (Hebert et al., 2012).

Virus production and infection

Nf2-expressing retroviruses were produced by cotransfecting 293T cells with pBABE constructs and the ψ2 packaging vector using the Fugene6 transfection reagent (Promega). The virus was harvested 24, 36, and 48 h after transfection. LDCs were infected with *Nf2*-expressing retroviruses, and stable cell lines were generated by selection in 5 µg/ml puromycin. For all experiments, an empty pBABE vector was used as a control. *Nf2^{WT}*-expressing adenoviruses were generated using the AdEasy system (Agilent Technologies) as previously described (Lallemand et al., 2003). Full-length mouse *Nf2* was subcloned into the pAdCMV shuttle vector under the control of a CMV promoter. The plasmid was digested with Pme1 and cotransformed into BJ5183 cells with the adenoviral backbone vector pAdEasy-1. Confirmed recombinant clones were linearized by Pac1 digestion to expose the viral inverted terminal repeats and transfected into 293A cells for production of adenovirus. The virus was harvested by lysis and concentration of virus-producing 293A cells. LDCs were infected 24 h before the start of the experiment to induce gene expression. For all experiments, an empty adenoviral vector was used as a control. shRNA-expressing lentiviruses were generated by cotransfecting 293T cells with pLKO-puro.1 vectors and the packaging vectors ΔVPR and VSVG. Viruses were harvested 24, 36, and 48 h after transfection. shSCR-, shNF2-, or shNF2/shEZR-expressing lentiviruses were stably expressed in Caco2 cells after selection in 10 µg/ml puromycin.

Antibodies

Primary antibodies against the following antigens were used in this study: 1:250 (D1D8; Cell Signaling Technology) anti-Merlin rabbit monoclonal antibody; 1:500 (C-18; Santa Cruz Biotechnology, Inc.) anti-Merlin rabbit polyclonal antibody; 1:1,000 anti–β-catenin mouse monoclonal antibody (BD); 1:500 anti–α-catenin mouse monoclonal antibody (7A4; Zymed); 1:500 anti–N-cadherin mouse monoclonal antibody (Transduction Labs); 1:500 anti–E-cadherin mouse monoclonal antibody (BD); 1:100 anti-Vinculin mouse monoclonal antibody (Sigma-Aldrich); 1:500 anti-nonmuscle Myosin IIA heavy chain rabbit polyclonal antibody (Covance); 1:500 anti-nonmuscle Myosin IIB heavy chain rabbit polyclonal antibody (Covance); anti–phospho-Myosin light chain 2 (serine 19) 1:100 rabbit polyclonal antibody (Cell Signaling Technology); 1:500 anti–ZO-1 rabbit polyclonal antibody (Life Technologies); 1:500 immunofluorescence and 1:1,000 Western blot anti-Ezrin mouse monoclonal antibody (Neomarkers); 1:100 anti-pERM rabbit polyclonal antibody (Cell Signaling Technology); and 1:2,000 actin (Sigma-Aldrich). F-actin was labeled with Alexa Fluor 488–phalloidin or Rhodamine-phalloidin (1:500; Life Technologies). Secondary antibodies were species-specific antibodies conjugated with Alexa Fluor 488, 555, or 647 for immunofluorescence (Life Technologies). DAPI was added to cells during the final wash to label the nuclei.

SPTM

EGF-conjugated polystyrene microspheres were used to track EGFR lateral mobility at the dorsal membrane of cells plated on 12-mm cov-

erslips. Bead binding was typically 0.5% of cells for BSA-labeled control beads and 3% (sixfold selectivity) for EGF-labeled beads. SPTM experiments were typically conducted in the presence of DMEM/10% FBS. Where indicated, SPTM was conducted in serum-free DMEM after overnight starvation after two PBS washes.

Cells were observed on a microscope (TE2000-E; Nikon) equipped with differential interference contrast optics using a 60× oil objective with an oil condenser (NA 1.4; Mirchev and Golan, 2001). Images of a single bead on individual cells were captured at 1,000 frames per second with a camera (Fastcam Super10K; Photron), and 2,000 frames were recorded. Video data were processed with MetaMorph software (Molecular Devices) and converted to trajectories. Trajectory data were analyzed using mean square displacement (MSD) analysis implemented in custom programs written in MATLAB (popall, popfunL, popfunN, sptload, and sptworkup; see supplemental materials; MathWorks). D_{macro} coefficients were calculated by fitting the initial third of the MSD versus time interval curve to the following equation: $MSD = 4D_{macro}t^{\alpha}$. Statistical significance was determined using a one-way analysis of variance (ANOVA) with multiple comparisons. Distinct populations of trajectories were identified by using a kernel density function to calculate a population density estimate based on the calculated D_{macro} parameter and determine the relative contributions of each subpopulation (Cairo et al., 2006).

For laser optical tweezers, the beam was supplied by a 1,064-nm neodymium-doped yttrium orthovanadate laser (Millennia IR; Spectra Physics). The beam was expanded and directed through steering optics consisting of a motorized gimbal mirror, used for moving the trap in the x and y directions (i.e., in the sample plane), and a lens on a motorized linear stage was used for positioning the trap in the z direction (i.e., perpendicular to the sample plane). A dichroic filter was used to introduce the beam into the microscope light path, and the beam was focused inside the sample volume by a 100/1.3 NA oil immersion objective. The sample was placed on a stage (XY-piezo; Physik Instrumente). Laser tweezer manipulation and data collection were managed through a custom-designed graphic user interface. Stage steering moved the cell in contact with the functionalized bead captured in the laser trap. The bead was held in contact with the cell membrane for 30 s to allow formation of ligand–receptor interactions. The trap was then turned off and the bead was allowed to diffuse freely. Trajectories of beads that remained attached to the cell were recorded and processed as described in the previous paragraph.

Polyacrylamide gel fabrication, collagen coating, and mechanical validation

Polyacrylamide solutions were prepared as previously described (Tse and Engler, 2010). In brief, acrylamide and bis-acrylamide were combined to desired concentrations in PBS. Stiffness was controlled by varying acrylamide (40% solution; Sigma-Aldrich) and *n*,*n*′-methylene-bis-acrylamide (2% solution; Sigma-Aldrich) concentrations; acrylamide/bis-acrylamide concentrations for soft or stiff gels were 5%/0.2% or 8%/0.5%, respectively. Glass coverslips were functionalized using 3-(trimethoxysilyl)propyl methacrylate (Sigma-Aldrich). Gels were molded into a 125 µm × 12 mm–diameter form using laser-cut adhesive-backed polyimide film (McMaster-Carr) attached to hydrophobic cyclic olefin copolymer slides (Pure Slides) and polymerized on functionalized coverslips using 1:100 volume 10% ammonium persulfate (Sigma-Aldrich) in H_2O as an initiator and 1:1,000 volume *n*,*n*,*n*′,*n*′-tetramethylethylenediamine (Sigma-Aldrich) as a catalyst. Sulfo-SANPAH (Thermo Fisher Scientific) was used to cross-link type I collagen (BD) to the surface of the gels. Sulfo-SANPAH was photoactivated using a UV cross-linker (UVP). Collagen was added at a concentration of 0.1 mg/ml and allowed to incubate at 4°C for 24 h.

Gel stiffness was determined by compressing a defined area of hydrated 5 mm × 25 mm–diameter gels a known distance and measuring the reactive force using a parallel plate mounted on a rheometer (Discovery Hybrid HR-3; TA Instruments). From these bulk measurements, highly linear force-displacement curves were obtained. Stress was calculated as the reactive force per unit area of the contact region of the gel and parallel plate. A least squares fitting was applied to a linear region of these curves corresponding to 7% strain, and the initial height of the gels was calculated by finding the indentation value corresponding to zero force along this curve. The elastic modulus, *E*, was obtained from this calculated initial height and the slope of the least squares fit.

Immunofluorescence microscopy and TR-EGF internalization assay

Cell confluence was defined as previously described (Curto et al., 2007). In brief, early confluent cells were defined as those plated on glass coverslips and allowed to grow until a monolayer formed (24–48 h). Late confluent cells were cultured for an additional 3–4 d after initial monolayer formation. Internalization of TR-EGF was measured as previously described (Curto et al., 2007). In brief, confluent monolayers were serum starved in DMEM/1% BSA for 2 h and then incubated for 30 min at 37°C with 2 µg/ml TR-EGF (Life Technologies). Cells were fixed in 4% paraformaldehyde in cytoskeletal stabilization buffer (10-mM Pipes, pH 6.8, 100-mM KCl, 300-mM sucrose, 2-mM EGTA, and 2-mM $MgCl_2$) for 15 min followed by permeabilization in 0.2% Triton X-100 in PBS for 10 min. Confocal images were captured on an inverted laser-scanning confocal microscope (LSM 710; Carl Zeiss) equipped with a 63× oil immersion objective (Plan Apochromat NA 1.4; Carl Zeiss). All samples were fixed and were imaged at room temperature. DAPI was excited with a 405-nm laser line of a diode laser. Green and red fluorescent probes (Alexa Fluor 488, Alexa Fluor 555, and Rhodamine) were excited with the 488-nm or 514-nm laser line of an argon laser, respectively. Far-red fluorescent probes (Alexa Fluor 647) were excited with the 633-nm laser line of a helium–neon laser. Two- or three-color fluorescent images were acquired as z stacks in sequential mode using Zen software (2012; Carl Zeiss).

Image analysis and statistics

ImageJ software (version 1.4; National Institutes of Health) was used for all image processing and analysis. For presented images, original z stack images were converted to maximum intensity projections, and a rolling ball background subtraction was applied to remove background signal. The application of lookup tables was used to produce final images. For fluorescent intensity analysis of cell–cell junctions, the region of interest tool was used to define areas of cell contact from vertex to vertex, as identified by β-catenin or α-catenin localization. Junction intensity was determined by applying a threshold mask to the region of interest and measuring the mean pixel intensity of the area within the mask. Cortical MyoIIA or Ezrin localization was measured by applying a thresholding mask and calculating the ratio of the area of MyoIIA or Ezrin localization to the total surface area of the cell, as bounded by F-actin or ZO-1 staining. The linearity index was determined similarly to the method described previously (Tokuda et al., 2014). Cell–cell junctions stained for either ZO-1 or F-actin were manually traced from vertex to vertex using either a freehand line or a straight line. The linearity index was calculated as the ratio of the length of the freehand line to the length of the straight line. The results were graphed as the mean ratio of freehand to straight line. TR-EGF internalization was quantified by using a thresholding mask to identify internalized TR-EGF vesicles. The number of vesicles per image was divided by the number of nuclei (as determined by DAPI staining). Data from all analyses were imported into Prism 6 software (GraphPad Software) for statistical analysis and plotting of graphs. The Mann-Whitney test was used to compare groups.

Online supplemental material

Fig. S1 shows that exogenous and endogenous Merlin regulate the lateral mobility and internalization of EGFR in a contact-dependent manner. Fig. S2 demonstrates that EGFR immobilization and inhibition of internalization occurs at the plasma membrane independently of sterol-rich membrane microdomains. Fig. S3 shows the localization of Merlin and AJ proteins in *Nf2*$^{-/-}$ *and Nf2*^{WT}-expressing LDCs. Fig. S4 shows that LDCs exhibit MyoIIA coalescence and Myosin-dependent regulation of TR-EGF internalization. Fig. S5 shows ectopic apical Ezrin localization and increased pERM levels in *Nf2*$^{-/-}$ LDCs, decreased Merlin and Ezrin levels in shNF2/shEzrin Caco2 cells, and that mitotic control Caco2 cells exhibit sinuous junctions and increased apical Ezrin. Table S1 lists the D_{macro} coefficients for EGFR under all experimental conditions tested. Table S2 lists all of the data for TR-EGF internalization under all experimental conditions tested. The following custom MATLAB programs were used to analyze trajectory data to determine MSD: popall loads the dataset and analyzes micro, macro, and α diffusion; popfunL carries out population analysis of SPTM results using log normal distribution analysis; popfunN carries out population analysis of SPTM results using normal distribution analysis; sptload reads all SPTM files and ensures the frame rates match; and sptworkup loads all trajectories into an array and analyzes them using MSD and subconfinement algorithms. Online supplemental material is available at http://www.jcb.org/cgi/content/full/jcb.201503081/DC1.

Acknowledgments

We thank present and past members of the McClatchey laboratory for valuable discussions; Helen Morrison, Marianne James, and Wayne Lencer for reagents; Mathew Ulman for assistance in the generation of polyacrylamide hydrogels; and Chris Chen and Nabeel El-Bardeesy for helpful comments.

This work was supported by grants from the National Institutes of Health (R01 CA113733 to A.I. McClatchey; R01 HL032854 to D.E. Golan; F31 GM78720 to Q. Baca; and T32 GM07306 to Z.S. Morris) and a fellowship from the Children's Tumor Foundation (to C. Chiasson-MacKenzie). A.I. McClatchey is the Patricia and Scott Eston MGH Reseach Scholar.

The authors declare no competing financial interests.

Submitted: 17 March 2015
Accepted: 1 September 2015

References

Avraham, R., and Y. Yarden. 2011. Feedback regulation of EGFR signalling: Decision making by early and delayed loops. *Nat. Rev. Mol. Cell Biol.* 12:104–117. http://dx.doi.org/10.1038/nrm3048

Benhamouche, S., M. Curto, I. Saotome, A.B. Gladden, C.H. Liu, M. Giovannini, and A.I. McClatchey. 2010. Nf2/Merlin controls progenitor homeostasis and tumorigenesis in the liver. *Genes Dev.* 24:1718–1730. http://dx.doi.org/10.1101/gad.1938710

Benjamin, J.M., A.V. Kwiatkowski, C. Yang, F. Korobova, S. Pokutta, T. Svitkina, W.I. Weis, and W.J. Nelson. 2010. αE-catenin regulates actin dynamics independently of cadherin-mediated cell–cell adhesion. *J. Cell Biol.* 189:339–352. http://dx.doi.org/10.1083/jcb.200910041

Boggiano, J.C., and R.G. Fehon. 2012. Growth control by committee: Intercellular junctions, cell polarity, and the cytoskeleton regulate Hippo signaling. *Dev. Cell.* 22:695–702. http://dx.doi.org/10.1016/j.devcel.2012.03.013

Buckley, C.D., J. Tan, K.L. Anderson, D. Hanein, N. Volkmann, W.I. Weis, W.J. Nelson, and A.R. Dunn. 2014. Cell adhesion. The minimal cadherin-catenin complex binds to actin filaments under force. *Science.* 346:1254211. http://dx.doi.org/10.1126/science.1254211

Cairo, C.W., R. Mirchev, and D.E. Golan. 2006. Cytoskeletal regulation couples LFA-1 conformational changes to receptor lateral mobility and clustering. *Immunity.* 25:297–308. http://dx.doi.org/10.1016/j.immuni.2006.06.012

Carreno, S., I. Kouranti, E.S. Glusman, M.T. Fuller, A. Echard, and F. Payre. 2008. Moesin and its activating kinase Slik are required for cortical stability and microtubule organization in mitotic cells. *J. Cell Biol.* 180:739–746. http://dx.doi.org/10.1083/jcb.200709161

Chua, J., R. Rikhy, and J. Lippincott-Schwartz. 2009. Dynamin 2 orchestrates the global actomyosin cytoskeleton for epithelial maintenance and apical constriction. *Proc. Natl. Acad. Sci. USA.* 106:20770–20775. http://dx.doi.org/10.1073/pnas.0909812106

Cole, B.K., M. Curto, A.W. Chan, and A.I. McClatchey. 2008. Localization to the cortical cytoskeleton is necessary for Nf2/merlin-dependent epidermal growth factor receptor silencing. *Mol. Cell. Biol.* 28:1274–1284. http://dx.doi.org/10.1128/MCB.01139-07

Curto, M., B.K. Cole, D. Lallemand, C.H. Liu, and A.I. McClatchey. 2007. Contact-dependent inhibition of EGFR signaling by Nf2/Merlin. *J. Cell Biol.* 177:893–903. http://dx.doi.org/10.1083/jcb.200703010

Dawes-Hoang, R.E., K.M. Parmar, A.E. Christiansen, C.B. Phelps, A.H. Brand, and E.F. Wieschaus. 2005. folded gastrulation, cell shape change and the control of myosin localization. *Development.* 132:4165–4178. http://dx.doi.org/10.1242/dev.01938

DuFort, C.C., M.J. Paszek, and V.M. Weaver. 2011. Balancing forces: Architectural control of mechanotransduction. *Nat. Rev. Mol. Cell Biol.* 12:308–319. http://dx.doi.org/10.1038/nrm3112

Dunagan, M., K. Chaudhry, G. Samak, and R.K. Rao. 2012. Acetaldehyde disrupts tight junctions in Caco-2 cell monolayers by a protein phosphatase 2A-dependent mechanism. *Am. J. Physiol. Gastrointest. Liver Physiol.* 303:G1356–G1364. http://dx.doi.org/10.1152/ajpgi.00526.2011

Fehon, R.G., A.I. McClatchey, and A. Bretscher. 2010. Organizing the cell cortex: The role of ERM proteins. *Nat. Rev. Mol. Cell Biol.* 11:276–287. http://dx.doi.org/10.1038/nrm2866

García-Sáez, A.J., and P. Schwille. 2007. Single molecule techniques for the study of membrane proteins. *Appl. Microbiol. Biotechnol.* 76:257–266. http://dx.doi.org/10.1007/s00253-007-1007-8

Gauthier, N.C., T.A. Masters, and M.P. Sheetz. 2012. Mechanical feedback between membrane tension and dynamics. *Trends Cell Biol.* 22:527–535. http://dx.doi.org/10.1016/j.tcb.2012.07.005

Giovannini, M., E. Robanus-Maandag, M. van der Valk, M. Niwa-Kawakita, V. Abramowski, L. Goutebroze, J.M. Woodruff, A. Berns, and G. Thomas. 2000. Conditional biallelic Nf2 mutation in the mouse promotes manifestations of human neurofibromatosis type 2. *Genes Dev.* 14:1617–1630.

Gladden, A.B., A.M. Hebert, E.E. Schneeberger, and A.I. McClatchey. 2010. The NF2 tumor suppressor, Merlin, regulates epidermal development through the establishment of a junctional polarity complex. *Dev. Cell.* 19:727–739. http://dx.doi.org/10.1016/j.devcel.2010.10.008

Hanahan, D., and R.A. Weinberg. 2011. Hallmarks of cancer: The next generation. *Cell.* 144:646–674. http://dx.doi.org/10.1016/j.cell.2011.02.013

Hansen, S.D., A.V. Kwiatkowski, C.Y. Ouyang, H. Liu, S. Pokutta, S.C. Watkins, N. Volkmann, D. Hanein, W.I. Weis, R.D. Mullins, and W.J. Nelson. 2013. αE-catenin actin-binding domain alters actin filament conformation and regulates binding of nucleation and disassembly factors. *Mol. Biol. Cell.* 24:3710–3720. http://dx.doi.org/10.1091/mbc.E13-07-0388

Hebert, A.M., B. DuBoff, J.B. Casaletto, A.B. Gladden, and A.I. McClatchey. 2012. Merlin/ERM proteins establish cortical asymmetry and centrosome position. *Genes Dev.* 26:2709–2723. http://dx.doi.org/10.1101/gad.194027.112

Hildebrand, J.D. 2005. Shroom regulates epithelial cell shape via the apical positioning of an actomyosin network. *J. Cell Sci.* 118:5191–5203. http://dx.doi.org/10.1242/jcs.02626

Huang, S., and D.E. Ingber. 2005. Cell tension, matrix mechanics, and cancer development. *Cancer Cell.* 8:175–176. http://dx.doi.org/10.1016/j.ccr.2005.08.009

James, M.F., J.M. Lelke, M. Maccollin, S.R. Plotkin, A.O. Stemmer-Rachamimov, V. Ramesh, and J.F. Gusella. 2008. Modeling NF2 with human arachnoidal and meningioma cell culture systems: NF2 silencing reflects the benign character of tumor growth. *Neurobiol. Dis.* 29:278–292. http://dx.doi.org/10.1016/j.nbd.2007.09.002

Jaqaman, K., and S. Grinstein. 2012. Regulation from within: The cytoskeleton in transmembrane signaling. *Trends Cell Biol.* 22:515–526. http://dx.doi.org/10.1016/j.tcb.2012.07.006

Kim, J.H., and A.R. Asthagiri. 2011. Matrix stiffening sensitizes epithelial cells to EGF and enables the loss of contact inhibition of proliferation. *J. Cell Sci.* 124:1280–1287. http://dx.doi.org/10.1242/jcs.078394

Kim, J.H., K. Kushiro, N.A. Graham, and A.R. Asthagiri. 2009. Tunable interplay between epidermal growth factor and cell–cell contact governs

the spatial dynamics of epithelial growth. *Proc. Natl. Acad. Sci. USA.* 106:11149–11153. http://dx.doi.org/10.1073/pnas.0812651106

Kraning-Rush, C.M., and C.A. Reinhart-King. 2012. Controlling matrix stiffness and topography for the study of tumor cell migration. *Cell Adhes. Migr.* 6:274–279. http://dx.doi.org/10.4161/cam.21076

Kunda, P., A.E. Pelling, T. Liu, and B. Baum. 2008. Moesin controls cortical rigidity, cell rounding, and spindle morphogenesis during mitosis. *Curr. Biol.* 18:91–101. http://dx.doi.org/10.1016/j.cub.2007.12.051

Kusumi, A., Y. Sako, and M. Yamamoto. 1993. Confined lateral diffusion of membrane receptors as studied by single particle tracking (nanovid microscopy). Effects of calcium-induced differentiation in cultured epithelial cells. *Biophys. J.* 65:2021–2040. http://dx.doi.org/10.1016/S0006-3495(93)81253-0

Lallemand, D., M. Curto, I. Saotome, M. Giovannini, and A.I. McClatchey. 2003. NF2 deficiency promotes tumorigenesis and metastasis by destabilizing adherens junctions. *Genes Dev.* 17:1090–1100. http://dx.doi.org/10.1101/gad.1054603

Lecuit, T., P.F. Lenne, and E. Munro. 2011. Force generation, transmission, and integration during cell and tissue morphogenesis. *Annu. Rev. Cell Dev. Biol.* 27:157–184. http://dx.doi.org/10.1146/annurev-cellbio-100109-104027

Leerberg, J.M., G.A. Gomez, S. Verma, E.J. Moussa, S.K. Wu, R. Priya, B.D. Hoffman, C. Grashoff, M.A. Schwartz, and A.S. Yap. 2014. Tension-sensitive actin assembly supports contractility at the epithelial zonula adherens. *Curr. Biol.* 24:1689–1699. http://dx.doi.org/10.1016/j.cub.2014.06.028

Lemmon, M.A., and J. Schlessinger. 2010. Cell signaling by receptor tyrosine kinases. *Cell.* 141:1117–1134. http://dx.doi.org/10.1016/j.cell.2010.06.011

Lenne, P.F., L. Wawrezinieck, F. Conchonaud, O. Wurtz, A. Boned, X.J. Guo, H. Rigneault, H.T. He, and D. Marguet. 2006. Dynamic molecular confinement in the plasma membrane by microdomains and the cytoskeleton meshwork. *EMBO J.* 25:3245–3256. http://dx.doi.org/10.1038/sj.emboj.7601214

Lidke, D.S., K.A. Lidke, B. Rieger, T.M. Jovin, and D.J. Arndt-Jovin. 2005. Reaching out for signals: Filopodia sense EGF and respond by directed retrograde transport of activated receptors. *J. Cell Biol.* 170:619–626. http://dx.doi.org/10.1083/jcb.200503140

Lien, W.H., V.I. Gelfand, and V. Vasioukhin. 2008. α–E-catenin binds to dynamitin and regulates dynactin-mediated intracellular traffic. *J. Cell Biol.* 183:989–997. http://dx.doi.org/10.1083/jcb.200805041

Luxenburg, C., H.A. Pasolli, S.E. Williams, and E. Fuchs. 2011. Developmental roles for Srf, cortical cytoskeleton and cell shape in epidermal spindle orientation. *Nat. Cell Biol.* 13:203–214. http://dx.doi.org/10.1038/ncb2163

Martin, A.C., and B. Goldstein. 2014. Apical constriction: Themes and variations on a cellular mechanism driving morphogenesis. *Development.* 141:1987–1998. http://dx.doi.org/10.1242/dev.102228

Martin, A.C., M. Kaschube, and E.F. Wieschaus. 2009. Pulsed contractions of an actin–myosin network drive apical constriction. *Nature.* 457:495–499. http://dx.doi.org/10.1038/nature07522

Maruthamuthu, V., B. Sabass, U.S. Schwarz, and M.L. Gardel. 2011. Cell-ECM traction force modulates endogenous tension at cell–cell contacts. *Proc. Natl. Acad. Sci. USA.* 108:4708–4713. http://dx.doi.org/10.1073/pnas.1011123108

McClatchey, A.I. 2014. ERM proteins at a glance. *J. Cell Sci.* 127:3199–3204. http://dx.doi.org/10.1242/jcs.098343

McClatchey, A.I., and R.G. Fehon. 2009. Merlin and the ERM proteins—regulators of receptor distribution and signaling at the cell cortex. *Trends Cell Biol.* 19:198–206. http://dx.doi.org/10.1016/j.tcb.2009.02.006

McClatchey, A.I., and A.S. Yap. 2012. Contact inhibition (of proliferation) redux. *Curr. Opin. Cell Biol.* 24:685–694. http://dx.doi.org/10.1016/j.ceb.2012.06.009

Mirchev, R., and D.E. Golan. 2001. Single-particle tracking and laser optical tweezers studies of the dynamics of individual protein molecules in membranes of intact human and mouse red cells. *Blood Cells Mol. Dis.* 27:143–147. http://dx.doi.org/10.1006/bcmd.2000.0367

Morris, Z.S., and A.I. McClatchey. 2009. Aberrant epithelial morphology and persistent epidermal growth factor receptor signaling in a mouse model of renal carcinoma. *Proc. Natl. Acad. Sci. USA.* 106:9767–9772. http://dx.doi.org/10.1073/pnas.0902031106

Nishimura, T., and M. Takeichi. 2008. Shroom3-mediated recruitment of Rho kinases to the apical cell junctions regulates epithelial and neuroepithelial planar remodeling. *Development.* 135:1493–1502. http://dx.doi.org/10.1242/dev.019646

Otani, T., T. Ichii, S. Aono, and M. Takeichi. 2006. Cdc42 GEF Tuba regulates the junctional configuration of simple epithelial cells. *J. Cell Biol.* 175:135–146. http://dx.doi.org/10.1083/jcb.200605012

Postic, C., and M.A. Magnuson. 2000. DNA excision in liver by an albumin-Cre transgene occurs progressively with age. *Genesis.* 26:149–150. http://dx.doi.org/10.1002/(SICI)1526-968X(200002)26:2<149::AID-GENE16>3.0.CO;2-V

Saxton, M.J., and K. Jacobson. 1997. Single-particle tracking: Applications to membrane dynamics. *Annu. Rev. Biophys. Biomol. Struct.* 26:373–399. http://dx.doi.org/10.1146/annurev.biophys.26.1.373

Takeichi, M. 2014. Dynamic contacts: Rearranging adherens junctions to drive epithelial remodelling. *Nat. Rev. Mol. Cell Biol.* 15:397–410. http://dx.doi.org/10.1038/nrm3802

Tokuda, S., T. Higashi, and M. Furuse. 2014. ZO-1 knockout by TALEN-mediated gene targeting in MDCK cells: Involvement of ZO-1 in the regulation of cytoskeleton and cell shape. *PLoS ONE.* 9:e104994. http://dx.doi.org/10.1371/journal.pone.0104994

Tse, J.R., and A.J. Engler. 2010. Preparation of hydrogel substrates with tunable mechanical properties. *In* Current Protocols in Cell Biology. John Wiley & Sons Inc., New York. http://dx.doi.org/10.1002/0471143030.cb1016s47

van der Flier, L.G., and H. Clevers. 2009. Stem cells, self-renewal, and differentiation in the intestinal epithelium. *Annu. Rev. Physiol.* 71:241–260. http://dx.doi.org/10.1146/annurev.physiol.010908.163145

Verma, S., S.P. Han, M. Michael, G.A. Gomez, Z. Yang, R.D. Teasdale, A. Ratheesh, E.M. Kovacs, R.G. Ali, and A.S. Yap. 2012. A WAVE2–Arp2/3 actin nucleator apparatus supports junctional tension at the epithelial zonula adherens. *Mol. Biol. Cell.* 23:4601–4610. http://dx.doi.org/10.1091/mbc.E12-08-0574

Viswanatha, R., P.Y. Ohouo, M.B. Smolka, and A. Bretscher. 2012. Local phosphocycling mediated by LOK/SLK restricts ezrin function to the apical aspect of epithelial cells. *J. Cell Biol.* 199:969–984. http://dx.doi.org/10.1083/jcb.201207047

Wakatsuki, T., B. Schwab, N.C. Thompson, and E.L. Elson. 2001. Effects of cytochalasin D and latrunculin B on mechanical properties of cells. *J. Cell Sci.* 114:1025–1036.

Wu, S.K., G.A. Gomez, M. Michael, S. Verma, H.L. Cox, J.G. Lefevre, R.G. Parton, N.A. Hamilton, Z. Neufeld, and A.S. Yap. 2014. Cortical F-actin stabilization generates apical–lateral patterns of junctional contractility that integrate cells into epithelia. *Nat. Cell Biol.* 16:167–178. http://dx.doi.org/10.1038/ncb2900

Yonemura, S., Y. Wada, T. Watanabe, A. Nagafuchi, and M. Shibata. 2010. α-Catenin as a tension transducer that induces adherens junction development. *Nat. Cell Biol.* 12:533–542. http://dx.doi.org/10.1038/ncb2055